Eur. Phys. J. Special Topics **160**, 127–138 (2008)
© EDP Sciences, Springer-Verlag 2008
DOI: 10.1140/epjst/e2008-00716-9

THE EUROPEAN PHYSICAL JOURNAL
SPECIAL TOPICS

XX model on the circle

A. De Pasquale[1], G. Costantini[1,2], P. Facchi[3,2], G. Florio[1,2], S. Pascazio[1,2], and K. Yuasa[4,5]

[1] Dipartimento di Fisica, Università di Bari, 70126 Bari, Italy
[2] Istituto Nazionale di Fisica Nucleare, Sezione di Bari, 70126 Bari, Italy
[3] Dipartimento di Matematica, Università di Bari, 70125 Bari, Italy
[4] Waseda Institute for Advanced Study, Waseda University, Tokyo 169-8050, Japan
[5] Department of Physics, Waseda University, Tokyo 169-8555, Japan

Abstract. We diagonalize the XX model with a finite number of spins and periodic boundary conditions. We solve for the ground state, focus on the rapidity of the convergence to the thermodynamic limit and study the features of multipartite entanglement.

1 Introduction

Recent advances in quantum information processing motivated a widespread interest for spin systems as models for quantum computers [1]. Spin chains are often studied, in particular in the thermodynamic limit [2–4], where one can neglect the contributions deriving from the finite size of the system, that scale like $O(1/N)$, with N the number of spins. However, due to experimental and theoretical difficulties, such as decoherence and/or imperfections in the quantum hardware, nowadays it is only possible to assemble and control the interaction of a small number of qubits (always less than 10). For this reason, it is extremely important to take into account all finite-size effects in the system Hamiltonian.

The investigation of the last few years has focused on entanglement [5] in diverse finite-size models, by means of direct diagonalization [6]. These studies were boosted by the recent discovery that entanglement can detect the presence of quantum phase transitions [7]. In this article we will study the finite-size 1D quantum XX model with periodic boundary conditions. We will exactly diagonalize the Hamiltonian by a Jordan-Wigner transformation followed by a deformed Fourier transform. Some of the results we will obtain were alluded to in the seminal article by Lieb et al. [3] and were discussed by Štelmachovič and Bužek [8] and very recently by Canosa and Rossignoli [9]. We will focus here on the features of the ground state and evaluate the "forerunners" of the critical points, as the quantum phase transition (QPT) occurs only in the thermodynamical limit. By introducing a finite-size parameter, we will show that the thermodynamical limit is very rapidly approached, so that a 10 qubit system already represents a very good approximation. Finally, we shall analyze the multipartite entanglement features of the finite-size ground state.

2 Exact diagonalization of the finite size XX model

2.1 Exact diagonalization of the Hamiltonian

The XX model for a collection of N qubits on a chain is described by the Hamiltonian

$$H = -J \sum_{i=0}^{N-1} \left(g\sigma_i^z + \frac{1}{2}\sigma_i^x \sigma_{i+1}^x + \frac{1}{2}\sigma_i^y \sigma_{i+1}^y \right), \tag{1}$$

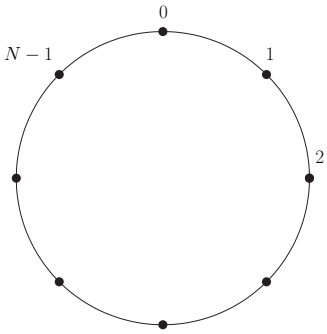

Fig. 1. A spin chain with periodic boundary conditions.

where J is a constant with dimensions of energy and g a dimensionless parameter proportional to the transverse magnetic field. We consider periodic boundary conditions (cyclic chain, see Fig. 1)

$$\sigma_0 = \sigma_N. \tag{2}$$

The usual diagonalization scheme is a two-step procedure based on the Jordan-Wigner (JW) transformation followed by a Fourier transform. The use of the JW transformation is based on the observation that there exists a unitary mapping between the Hilbert space of N qubits $(\mathbb{C}^2)^{\otimes N}$ and the antisymmetric Fock space $\mathcal{F}_-(\mathbb{C}^N)$ of spinless fermions on N orbitals. We can define annihilation and creation operators for $\mathcal{F}_-$,

$$c_i = \left(\prod_{0\le j<i} \sigma_j^z\right)\sigma_i^- = e^{\mathrm{i}\pi\mathbf{n}_{i\downarrow}}\sigma_i^-, \qquad c_i^\dagger = \left(\prod_{0\le j<i} \sigma_j^z\right)\sigma_i^+ = e^{\mathrm{i}\pi\mathbf{n}_{i\downarrow}}\sigma_i^+, \quad \forall i \in \mathbb{Z}_N, \tag{3}$$

where $\sigma_i^\pm = (\sigma_i^x \pm \mathrm{i}\sigma_i^y)/2$, $\mathbb{Z}_N = \{0, 1, \ldots, N-1\}$, and $\mathbf{n}_{i\downarrow}$ is the number operator counting the holes between 0 and $i-1$,

$$\mathbf{n}_{i\downarrow} = \sum_{j=0}^{i-1}(1 - \sigma_j^+\sigma_j^-) = \sum_{j=0}^{i-1}\sigma_j^-\sigma_j^+. \tag{4}$$

It can be shown that the JW operators satisfy anticommutation relations

$$\{c_i, c_j\} = 0, \quad \{c_i^\dagger, c_j^\dagger\} = 0, \quad \{c_i, c_j^\dagger\} = \delta_{ij}, \quad \forall i, j \in \{0, 1, \ldots, N-1\}, \tag{5}$$

whereas the corresponding Pauli operators anticommute only on site:

$$\{\sigma_i^\pm, \sigma_j^\pm\} = 0 \qquad \text{for} \quad i = j, \quad [\sigma_i^\pm, \sigma_j^\pm] = 0 \qquad \text{for} \quad i \neq j. \tag{6}$$

The periodic boundary conditions assigned to the cyclic chain do not hold in general for the fermionic operators c_i; indeed, by prolonging (3) up to $i = N$ we would obtain

$$c_0 = \sigma_0^-, \qquad c_N = e^{\mathrm{i}\pi\mathbf{n}_\downarrow}\sigma_N^- = e^{\mathrm{i}\pi\mathbf{n}_\downarrow}\sigma_0^- = e^{\mathrm{i}\pi\mathbf{n}_\downarrow}c_0, \tag{7}$$

where $\mathbf{n}_\downarrow = \mathbf{n}_{N\downarrow}$ is the number operator that counts the total number of spins down (and the number of holes), from 0 to $N-1$. As a consequence, the Hamiltonian written in terms of the JW operators is characterized by the presence of a boundary term:

$$H = -J\left[\sum_{j=0}^{N-1} g(1 - 2c_jc_j^\dagger) + \sum_{j=0}^{N-2}(c_jc_{j+1}^\dagger + c_{j+1}c_j^\dagger) + (e^{\mathrm{i}\pi(\mathbf{n}_\downarrow+1)} - 1)(c_{N-1}c_0^\dagger + c_0c_{N-1}^\dagger)\right]. \tag{8}$$

In the thermodynamic limit [3,4] the XX Hamiltonian is diagonalized by introducing the discrete Fourier transform

$$c_j = \frac{1}{\sqrt{N}} \sum_{k=0}^{N-1} e^{\frac{2\pi i k j}{N}} \hat{c}_k, \qquad \forall j \in \mathbb{Z}_N \tag{9}$$

and neglecting the last term in (8), since its contribution scales like $O(1/N)$. We intend to evaluate the corrections due to the finite size of the chain.

The main difficulty introduced by the boundary term in the Hamiltonian (8) is that it breaks the periodicity of the JW operators, due to the arbitrary dependence of the phase $e^{\mathrm{i}\pi \mathbf{n}_{i\downarrow}}$ on the ordering of the spin on the circle. This phase clearly depends on the state the Hamiltonian H is applied to. However, notice that the parity of the spin-down number operator is conserved (although not so the number operator itself)

$$[e^{\mathrm{i}\pi \mathbf{n}_\downarrow}, H] = 0. \tag{10}$$

Therefore, let us consider the parity operator

$$\mathcal{P} = e^{\mathrm{i}\pi(\mathbf{n}_\downarrow + 1)} \tag{11}$$

and the spectral decomposition of the number operator $\mathbf{n}_\downarrow$,

$$\mathbf{n}_\downarrow = \sum_{n_\downarrow=0}^{N} n_\downarrow |n_\downarrow\rangle\langle n_\downarrow|, \tag{12}$$

where $|n_\downarrow\rangle$ is the eigenstate of $\mathbf{n}_\downarrow$ belonging to the eigenvalue $n_\downarrow$. In this basis the parity operator can be written as:

$$\mathcal{P} = e^{\mathrm{i}\pi(\mathbf{n}_\downarrow+1)} \sum_{n_\downarrow=0}^{N} |n_\downarrow\rangle\langle n_\downarrow| = P_+ - P_-, \tag{13}$$

where

$$P_+ = \sum_{n_\downarrow \text{ odd}} |n_\downarrow\rangle\langle n_\downarrow|, \qquad P_- = \sum_{n_\downarrow \text{ even}} |n_\downarrow\rangle\langle n_\downarrow| \tag{14}$$

are the projection operators associated to the eigenvalues ± 1 of $\mathcal{P}$, respectively. Due to Eq. (10), the Hamiltonian preserves the parity sectors and can be decomposed as

$$H = P_+ H P_+ + P_- H P_- = H^{(+)} + H^{(-)}. \tag{15}$$

The analysis can then be separately performed in the two parity sectors, where $\mathcal{P}$ acts as a c-number.

Let us define a deformed Fourier transform

$$c_j = \frac{1}{\sqrt{N}} e^{\frac{2\pi i \alpha_j}{N}} \sum_{k=0}^{N-1} e^{\frac{2\pi i k j}{N}} \hat{c}_k, \tag{16}$$

where we added a position dependent phase α_j ($j \in \mathbb{Z}_N$ denoting the site). The anticommutation relations for $\hat{c}_k$ still hold:

$$\{\hat{c}_k, \hat{c}_{k'}\} = 0, \qquad \{\hat{c}_k^\dagger, \hat{c}_{k'}^\dagger\} = 0, \qquad \{\hat{c}_k, \hat{c}_{k'}^\dagger\} = \delta_{kk'}. \tag{17}$$

The phase $e^{\frac{2\pi i \alpha_j}{N}}$ can be determined by imposing that the last term of Eq. (8), after Fourier transform, has the same form of the other $N-1$ terms: namely we require that the following two expressions,

$$c_j c_{j+1}^\dagger = e^{\frac{2\pi i \alpha_j}{N}} e^{-\frac{2\pi i \alpha_{j+1}}{N}} \frac{1}{N} \sum_{k=0}^{N-1} \sum_{k'=0}^{N-1} e^{\frac{2\pi i j k}{N}} e^{-\frac{2\pi i (j+1) k'}{N}} \hat{c}_k \hat{c}_{k'}^\dagger \tag{18}$$

and

$$\begin{aligned} e^{\mathrm{i}\pi(\mathbf{n}_\downarrow+1)}c_{N-1}c_0^\dagger &= e^{\mathrm{i}\pi(\mathbf{n}_\downarrow+1)}e^{\frac{2\pi\mathrm{i}\alpha_{N-1}}{N}}e^{-\frac{2\pi\mathrm{i}\alpha_0}{N}}\frac{1}{N}\sum_{k=0}^{N-1}\sum_{k'=0}^{N-1}e^{\frac{2\pi\mathrm{i}(N-1)k}{N}}\hat{c}_k\hat{c}_{k'}^\dagger \\ &= e^{\mathrm{i}\pi(\mathbf{n}_\downarrow+1)}e^{\frac{2\pi\mathrm{i}\alpha_{N-1}}{N}}e^{-\frac{2\pi\mathrm{i}\alpha_0}{N}}\frac{1}{N}\sum_{k=0}^{N-1}\sum_{k'=0}^{N-1}e^{\frac{2\pi\mathrm{i}(N-1)k}{N}}e^{-\frac{2\pi\mathrm{i}Nk'}{N}}\hat{c}_k\hat{c}_{k'}^\dagger, \end{aligned} \tag{19}$$

have the same phase. It follows that

$$e^{\frac{2\pi\mathrm{i}(\alpha_j-\alpha_{j+1})}{N}} = e^{\mathrm{i}\pi(\mathbf{n}_\downarrow+1)}e^{\frac{2\pi\mathrm{i}(\alpha_{N-1}-\alpha_0)}{N}}. \tag{20}$$

The solution is given by

$$\alpha_j = j\alpha + \alpha_0, \tag{21}$$

where α satisfies the equation

$$e^{2\pi\mathrm{i}\alpha} = e^{\mathrm{i}\pi(\mathbf{n}_\downarrow+1)}. \tag{22}$$

On the other hand, the phase of the first site α_0 is a free parameter. The two solutions in the two parity sectors are

$$\alpha = \begin{cases} 0 \bmod N & \text{if} \quad \mathcal{P}=+1 \qquad (n_\downarrow \text{ odd}), \\ \frac{1}{2} \bmod N & \text{if} \quad \mathcal{P}=-1 \qquad (n_\downarrow \text{ even}). \end{cases} \tag{23}$$

Summarizing, by using the (sector dependent) deformed Fourier transform

$$c_j = \frac{1}{\sqrt{N}}e^{\frac{2\pi\mathrm{i}\alpha_0}{N}}e^{\frac{2\pi\mathrm{i}\alpha j}{N}}\sum_{k=0}^{N-1}e^{\frac{2\pi\mathrm{i}kj}{N}}\hat{c}_k \tag{24}$$

and substituting into Eq. (8) we obtain

$$H = -2J\sum_{k=0}^{N-1}\left(\hat{c}_k^\dagger\hat{c}_k - \frac{1}{2}\right)\left[g - \cos\left(2\pi\frac{\alpha+k}{N}\right)\right], \tag{25}$$

where α is given by (23). In this way, H is diagonalized and the boundary term removed. Therefore, the Hamiltonian is given by (15) with

$$H^{(+)} = -2JP_+\sum_{k=0}^{N-1}\left(\hat{c}_k^\dagger\hat{c}_k - \frac{1}{2}\right)\left[g - \cos\left(2\pi\frac{k}{N}\right)\right]P_+, \tag{26}$$

$$H^{(-)} = -2JP_-\sum_{k=0}^{N-1}\left(\hat{c}_k^\dagger\hat{c}_k - \frac{1}{2}\right)\left[g - \cos\left(2\pi\frac{k}{N}+\frac{\pi}{N}\right)\right]P_-. \tag{27}$$

2.2 Energy spectrum

In this section we will focus on the spectrum of the system. We shall set henceforth $J = 1$. The state with no fermions has an energy density that is independent of α and of the number of sites N. Indeed, from Eq. (25),

$$\varepsilon_{\mathrm{vac}}(g) = \frac{E_{\mathrm{vac}}(g)}{N} = \frac{1}{N}\sum_{k=0}^{N-1}\left[g - \cos\left(2\pi\frac{\alpha+k}{N}\right)\right] = g. \tag{28}$$

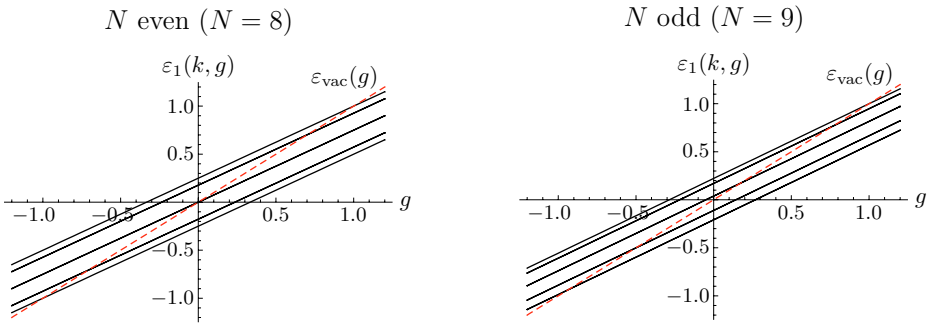

Fig. 2. Single particle spectra $\varepsilon_1(k,g)$ (solid lines) and vacuum density energies $\varepsilon_{\rm vac}(g)$ (dashed lines). Different lines correspond to different $k \in \mathbb{Z}_N$ according to (29).

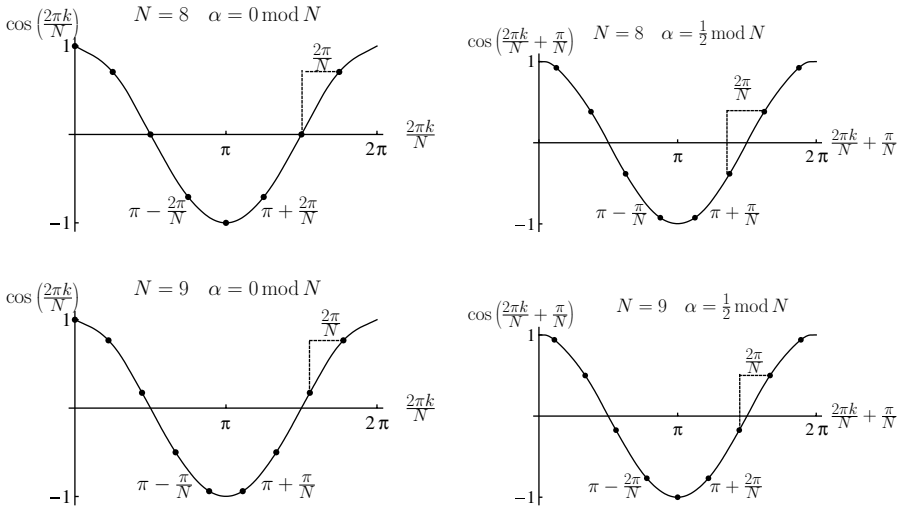

Fig. 3. Plot of $\cos[2\pi(\alpha+k)/N]$, $k \in \mathbb{Z}_N$ for $N = 8, 9$ and $\alpha = 0 \mod N$, $\frac{1}{2} \mod N$.

If we add one fermion the energy density reads

$$\varepsilon_1(k,g) = \varepsilon_{\rm vac}(g) - \frac{2}{N}\left[g - \cos\left(2\pi\frac{\alpha+k}{N}\right)\right], \tag{29}$$

where α depends on N:

$$\begin{cases} N \text{ even} \Rightarrow N-1 \text{ odd} & \Rightarrow \quad \alpha = 0 \mod N, \\ N \text{ odd} \Rightarrow N-1 \text{ even} & \Rightarrow \quad \alpha = \frac{1}{2} \mod N. \end{cases} \tag{30}$$

In Fig. 2 we represent the single particle energy spectra corresponding to $N = 8$ and 9 sites (representative of an even/odd number of fermionic sites, respectively). Different curves are parametrized by $k \in \mathbb{Z}_N$ and one notices the presence of degeneracies in both cases. Since we are interested in the ground state of the system, we focus on the lowest energy levels and consider the values assumed by the function $\cos[2\pi(\alpha+k)/N]$ in the four possible cases [2 parities of number of sites N and 2 values of α as in Eq. (23)], as shown in Fig. 3. Notice that these results can be described in terms of regular polygons inscribed into a circle of unit radius, see Fig. 4.

From Fig. 3 one obtains the values of k that minimize the energy per site; in the 1-particle sector one has

$$\begin{cases} N \text{ even} & \Rightarrow \quad \alpha = 0 \mod N \Rightarrow k = \frac{N}{2}, \\ N \text{ odd} & \Rightarrow \quad \alpha = \frac{1}{2} \mod N \Rightarrow k = \frac{N-1}{2}. \end{cases} \tag{31}$$

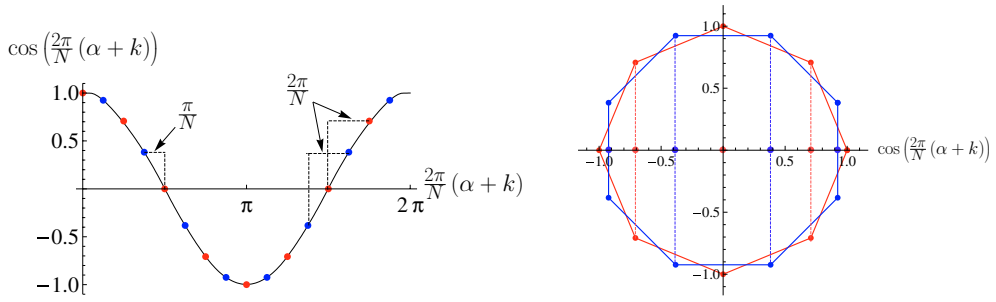

Fig. 4. (Color online) left: plot of $\cos[2\pi(\alpha+k)/N]$, $k \in \mathbb{Z}_N$ with $\alpha = 0 \bmod N$ (red) and $\alpha = \frac{1}{2} \bmod N$ (blue), for $N = 8$. Right: geometrical description of $\cos[2\pi(\alpha + k)/N]$.

Similarly, in the 2-particle sector the minimum energy is at

$$\begin{cases} N \text{ even} & \Rightarrow \quad \alpha = \frac{1}{2} \bmod N \Rightarrow \{k_1, k_2\} = \left\{\frac{N}{2} - 1, \frac{N}{2}\right\}, \\ N \text{ odd} & \Rightarrow \quad \alpha = 0 \bmod N \Rightarrow \{k_1, k_2\} = \left\{\frac{N-1}{2}, \frac{N+1}{2}\right\}. \end{cases} \tag{32}$$

As a result, the general expression of the lowest energy levels in the different n-particle sectors does not depend on the parity of N. For n fermions, one gets

$$\varepsilon_n^{\min}(g) = g\left(1 - \frac{2n}{N}\right) - \frac{2}{N}\frac{\sin(n\pi/N)}{\sin(\pi/N)}. \tag{33}$$

In Fig. 5 we plot the lowest energy levels corresponding to $0 \leq n \leq N$ for $N = 8$ sites. The intersections of levels corresponding to n and $n + 1$ fermions (starting from $n = 0$) define the *level crossing points* or *quantum critical points* g_c, where an excited level and the ground state are interchanged. The analytic expression of the critical points is easily obtained by the condition $\varepsilon_n^{\min}(g_c) = \varepsilon_{n+1}^{\min}(g_c)$. We find

$$g_c(n) = \frac{\sin(n\pi/N) - \sin[(n+1)\pi/N]}{\sin(\pi/N)}, \qquad 0 \leq n \leq N. \tag{34}$$

As a consequence, the ground-state energy per site is

$$\varepsilon_{\rm gs}(g) = g\left(1 - \frac{2n}{N}\right) - \frac{2}{N}\frac{\sin(n\pi/N)}{\sin(\pi/N)} \quad \text{with} \quad g \in (g_c(n-1), g_c(n)), \tag{35}$$

with $0 \leq n \leq N + 1$ and $g_c(-1) = -\infty$, $g_c(N + 1) = +\infty$. Thus, for $g \in (g_c(n - 1), g_c(n))$, the ground state contains n fermions. Note that $g_c(0) = -1$ and $g_c(N) = +1$, independently on N.

In the thermodynamic limit the critical points correspond to the QPT. In order to study the properties of the ground state in this limit, we evaluate the envelope of the lowest-energy levels. This is obtained by the equation

$$\frac{\partial \varepsilon_n^{\min}(g)}{\partial n} = 0 \quad \Rightarrow \quad n(g) = \frac{N}{\pi}\arccos(-g\chi_N), \tag{36}$$

where

$$\chi_N \equiv \frac{\sin(\pi/N)}{\pi/N} \tag{37}$$

is a *finite-size parameter* depending on the number N of sites in the chain. The envelope is obtained by plugging $n(g)$ from Eq. (36) into Eq. (35). By noting that $n = 0$ for $g \leq -1/\chi_N$ while $n = N$ for $g \geq 1/\chi_N$, one gets

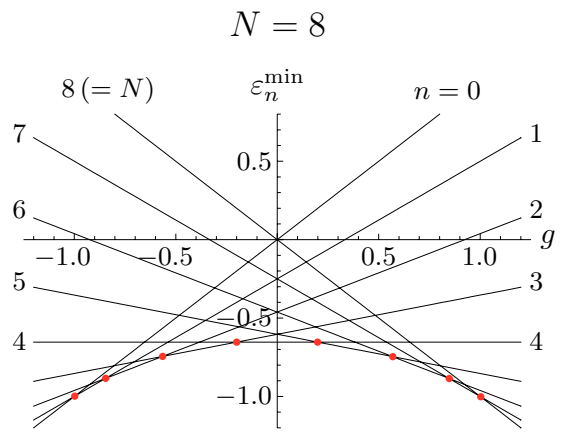

Fig. 5. Lowest-energy levels $\varepsilon_n^{\min}(g)$ for different number of fermions n; the intersection between the energy levels corresponding to n and $n+1$ fermions (starting from $n=0$) are the quantum critical points (dots).

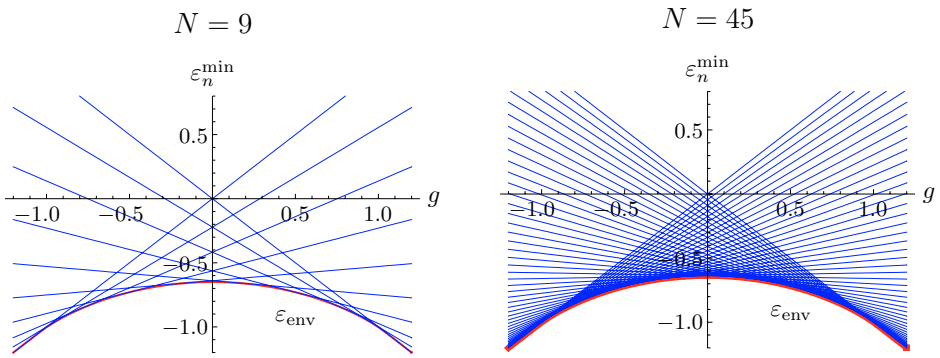

Fig. 6. Ground-state envelopes $\varepsilon_{\rm env}(g)$ for $N=9$ and 45 sites.

$$\varepsilon_{\rm env}(g) = \begin{cases} g\left(1-\dfrac{2}{\pi}\arccos(-g\chi_N)\right) - \dfrac{2}{\pi}\dfrac{\sqrt{1-g^2\chi_N^2}}{\chi_N} & \text{for} \quad |g| < \dfrac{1}{\chi_N}, \\ -|g| & \text{for} \quad |g| > \dfrac{1}{\chi_N}. \end{cases} \tag{38}$$

It is easy to see that the envelope and its first derivative are continuous functions at $|g| = 1/\chi_N$, whereas the second derivative

$$\frac{{\rm d}^2\varepsilon_{\rm env}(g)}{{\rm d}g^2} = \begin{cases} -\dfrac{2}{\pi}\dfrac{\chi_N}{\sqrt{1-g^2\chi_N^2}} & \text{for} \quad |g| < \dfrac{1}{\chi_N}, \\ 0 & \text{for} \quad |g| > \dfrac{1}{\chi_N}. \end{cases} \tag{39}$$

diverges to $-\infty$, for $|g| \uparrow 1/\chi_N$.

In Fig. 6 we plot the lowest-energy levels and the ground-state envelopes for $N=9$ and 45 sites. Notice that the scales of the energy and magnetic field are similar. This result is confirmed in Fig. 7, where we plot the envelopes for $N=9$ and 45; their difference is negligible if compared to the envelope for $N=5$, which shows that $N=9$ is already a good approximation of the thermodynamical limit.

It is interesting to evaluate the finite-size effects. This can be done by considering the dependence of χ_N on N. We plot this function in Fig. 8 (left). For $N > 10$, $\chi_N \simeq 1$ with

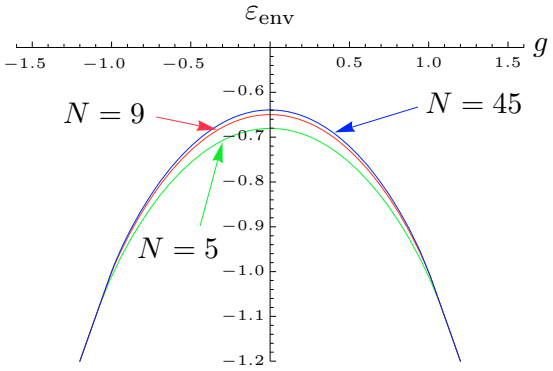

Fig. 7. Ground-state envelopes $\varepsilon_{\rm env}(g)$ for $N = 5$, 9, and 45 sites.

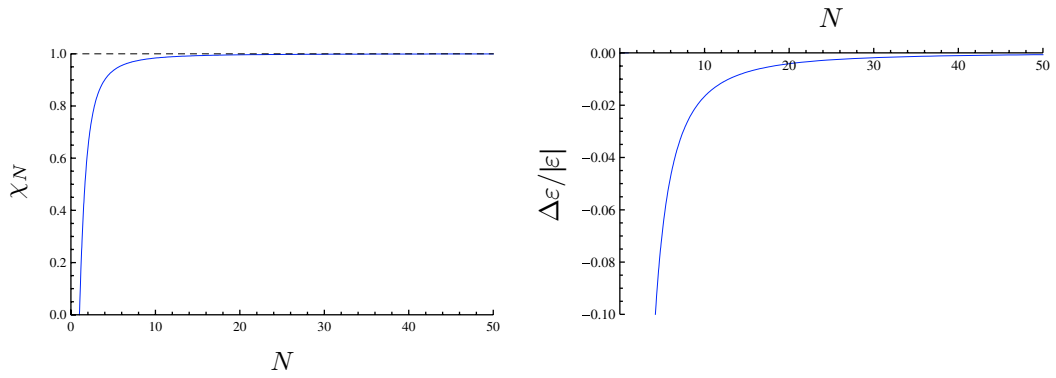

Fig. 8. Finite-size parameter χ_N (left) and relative error $\Delta\varepsilon/|\varepsilon|$ (right) for $N = 1, \ldots, 50$.

excellent approximation. We can obtain further information by looking at the thermodynamic limit of the envelope (38),

$$\varepsilon_\infty(g) = \lim_{N\to\infty} \varepsilon_{\rm env}(g) = \begin{cases} g\left(1 - \frac{2}{\pi}\arccos(-g)\right) - \frac{2}{\pi}\sqrt{1-g^2} & \text{for} \quad |g| \le 1, \\ -|g| & \text{for} \quad |g| \ge 1, \end{cases} \tag{40}$$

which is nothing but the ground state energy density of the thermodynamic system. The relative error reads (for $g = 0$)

$$\frac{\Delta\varepsilon}{|\varepsilon|} = \frac{\varepsilon_{\rm env}(0) - \varepsilon_\infty(0)}{|\varepsilon_\infty(0)|} = -\left(\frac{1}{\chi_N} - 1\right) \sim -\frac{1}{3!}\left(\frac{\pi}{N}\right)^2 \quad \text{for} \quad N \to \infty. \tag{41}$$

It is interesting to notice that the relative error is $O(1/N^2)$, which is better than what one naively expects, see comment after Eq. (9).

Figure 8 (right) confirms this result. The effect of the finite size of the chain can be neglected already for a relatively small number of sites.

2.3 Ground state revisited

It is interesting to reinterpret the ground state of the chain in terms of spins. For $g \le -1$ the ground state is the state with no fermions. By definition, this corresponds to all spins down (antiparallel to the z axis) in the chain

$$|\psi_0\rangle = |\downarrow\rangle|\downarrow\rangle \cdots |\downarrow\rangle. \tag{42}$$

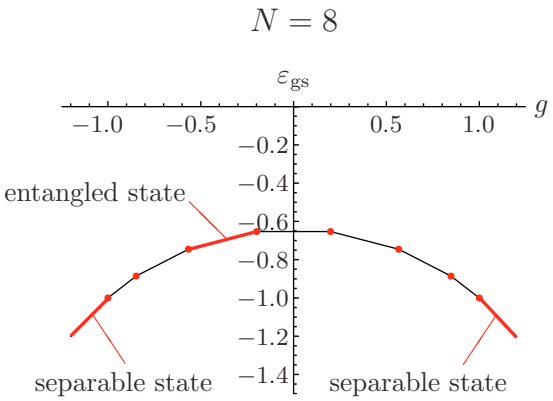

Fig. 9. Classification of the ground states in terms of entanglement ($N = 8$).

This means that for strong magnetic fields the interaction between the field and the spins is larger than that among the spins in the xy plane.

As the magnetic field tends to zero, the number of spins in the down state decreases and the general expression of the ground state for $g \in [g_c(n-1), g_c(n)]$ is given by

$$\begin{aligned}|\psi_n\rangle &= \frac{1}{N}\sum_{j_1<j_2<\cdots<j_n}\Big[\lambda_{j_1,j_2,\ldots,j_n}\sigma_{j_1}^{+}\sigma_{j_2}^{+}\cdots\sigma_{j_n}^{+}(\sigma_0^z)^n(\sigma_1^z)^n\cdots(\sigma_{j_1-1}^z)^n \\ &\times(\sigma_{j_1}^z)^{n-1}(\sigma_{j_1+1}^z)^{n-1}\cdots(\sigma_{j_2-1}^z)^{n-1}(\sigma_{j_2}^z)^{n-2}(\sigma_{j_2+1}^z)^{n-2}\cdots(\sigma_{j_3-1}^z)^{n-2}\cdots\sigma_{j_n-1}^z\Big] \\ &\times|\downarrow\rangle_0|\downarrow\rangle_1\cdots|\downarrow\rangle_{N-1} \\ &= \frac{1}{N}\sum_{j_1<j_2<\cdots<j_n}\Big[\lambda_{j_1,j_2,\ldots,j_n}(-1)^{nj_1}(-1)^{(n-1)(j_2-j_1)}(-1)^{(n-2)(j_3-j_2)}\cdots(-1)^{j_n-j_{n-1}}\Big] \\ &\times|\downarrow\rangle_0\cdots|\uparrow\rangle_{j_1}\cdots|\uparrow\rangle_{j_2}\cdots|\uparrow\rangle_{j_n}\cdots|\downarrow\rangle_{N-1}, \end{aligned} \tag{43}$$

where $\lambda_{j_1,j_2,\ldots,j_n}$ is the sum over all permutations $\{1,2,\ldots,n\} \to \{p_1,p_2,\ldots,p_n\}$

$$\lambda_{j_1,j_2,\ldots,j_n} = \sum_p (-1)^p e^{\frac{2\pi \mathrm{i}}{N}(k_1 j_{p_1}+k_2 j_{p_2}+\cdots+k_n j_{p_n})}. \tag{44}$$

Note that in this case the state of the system cannot be written as a tensor product and $|\psi_n\rangle$ is entangled. When the magnetic field is very strong and positive $g \geq 1$ (parallel to the z axis) all spins are aligned along its direction and the state of the chain is

$$|\psi_N\rangle = |\uparrow\rangle|\uparrow\rangle\cdots|\uparrow\rangle. \tag{45}$$

These properties are summarized in Fig. 9. We will analyze the entanglement structure for a finite-size chain in the following section.

3 Multipartite entanglement of the ground state

3.1 Probability density function characterization of multipartite entanglement

The evaluation of the entanglement stored in the ground states of quantum spin chains has become a central problem in this field of research. The study of the entanglement properties of the ground state usually explores the link between quantum phase transitions and entanglement generation and previous research mainly focused on the thermodynamic limit [7].

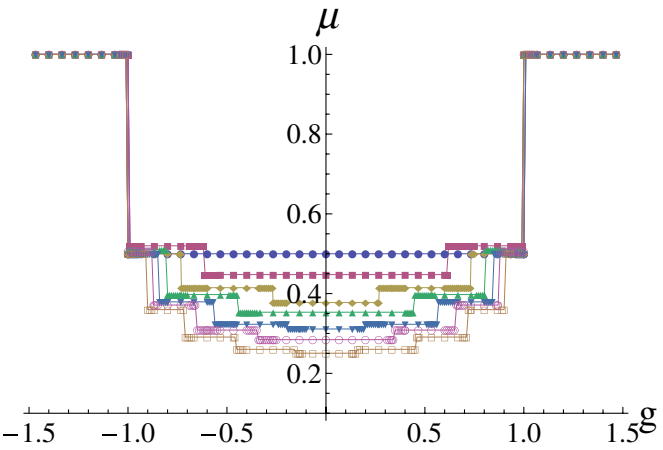

Fig. 10. Average μ of π_{AB} over all balanced bipartitions for the XX chain with periodic boundary conditions, with $N = 4$ (full circles), 5 (full squares), 6 (full diamonds), 7 (full triangles), 8 (full reverse triangles), 9 (open circles), 10 (open squares).

One can use several measures of entanglement [10]. A typical approach consists in considering a given bipartition and evaluating the bipartite entanglement (in terms of the von Neumann entropy, the linear entropy, the purity, or in general a well defined entanglement monotone [5]). A possible approach to multipartite entanglement is to analyze the statistical properties of bipartite entanglement over all balanced bipartitions (each part consisting of one half of the chain) [11]. This characterization has been applied to the 1D quantum Ising model in a transverse field, yielding interesting results [12].

We will characterize in a similar way the multipartite entanglement of the XX chain. Consider a chain of N spins and consider a partition in two subsystems A and B, made up of N_A and N_B qubits ($N_A + N_B = N$), respectively. For definiteness we assume $N_A \leq N_B$. The total Hilbert space is the tensor product $\mathcal{H} = \mathcal{H}_A \otimes \mathcal{H}_B$ with dimensions $\dim \mathcal{H}_A = 2^{N_A}$, $\dim \mathcal{H}_B = 2^{N_B}$, and $\dim \mathcal{H} = 2^{N_A+N_B} = 2^N$.

Let us denote the ground state by $|\psi_{\rm gs}\rangle$ and consider the purity of subsystem A (which equals that of subsystem B)

$$\pi_{AB}(|\psi_{\rm gs}\rangle) = {\rm Tr}_A \rho_A^2, \qquad \rho_A = {\rm Tr}_B \rho, \qquad \rho = |\psi_{\rm gs}\rangle\langle\psi_{\rm gs}|, \tag{46}$$

${\rm Tr}_A$ (${\rm Tr}_B$) being the partial trace over subsystem A (B), and take it as a measure of the bipartite entanglement between A and B. We note that

$$2^{-N_A} \leq \pi_{AB} \leq 1, \tag{47}$$

where the minimum (maximum) value is obtained for a completely mixed (pure) state ρ_A. Therefore, a smaller value of π_{AB} corresponds to a more entangled bipartition (A, B). π_{AB} will depend on the bipartition and entanglement will be distributed in a different way among all possible bipartitions. The key idea is that the average of π_{AB}, denoted by μ, measures the amount of entanglement (the smaller μ, the larger the entanglement), whereas the standard deviation σ measures how well this entanglement is distributed among bipartitions. Clearly, if the distribution function π_{AB} is not very regular, higher moments will be necessary in order to properly characterize it.

3.2 Average and standard deviation of the distribution

We numerically evaluated the distribution of bipartite entanglement for the finite-size XX model on the circle. In Fig. 10 we plot the average entanglement μ over balanced bipartitions versus the coupling g (for $N = 4, \ldots, 10$ sites).

Note that, as expected, the maximum entanglement is reached at $g = 0$. Moreover, the larger the system, the smaller μ. An interesting peculiarity of the XX model, at variance with

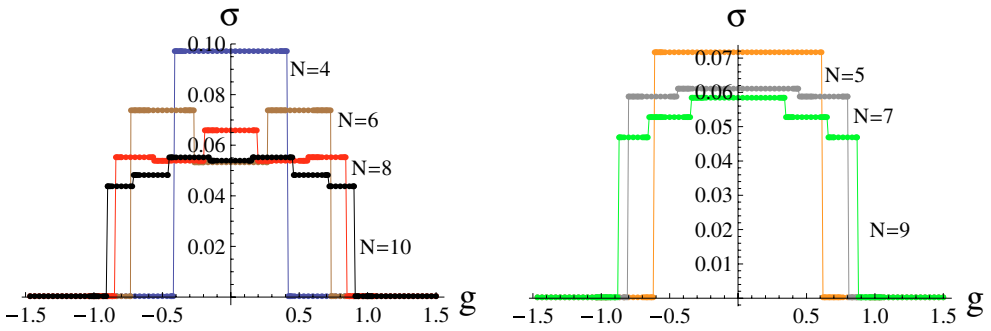

Fig. 11. Standard deviation σ of π_{AB} over all balanced bipartitions for the XX chain with periodic boundary conditions, with an even(left) and an odd (right) number of sites. (Left) $N = 4$ (full circles), 6 (full squares), 8 (full diamonds), 10 (full triangles). (Right) $N = 5$ (full circles), 7 (full squares), 9 (full diamonds).

the Ising chain [12], is that $\mu(g)$ is not continuous: we observe jumps between plateaux. These jumps correspond to the level crossing points defined in Eq. (34). In particular, for $|g| > 1$, the ground state of the model is completely factorized and, consequently, we have no entanglement ($\mu = 1$). The largest jump is found at $|g| = 1$, where $\mu \simeq 0.5$ for all N.

The standard deviation of the distribution is plotted in Fig. 11. We displayed separately the cases N even (left) and odd (right). Also in this case we observe a stepwise behavior, depending on the number of fermions in the ground state. For odd N the maximum of σ tends to decrease for a larger chain: the curves are monotone for $-1 \leq g \leq 0$ and $0 \leq g \leq 1$. On the other hand, for even N, σ shows a more complicated structure; the curves are not monotone. The maximum is not a decreasing function of the size (for $N = 8$ it is larger than for $N = 6$). As a general trend, however, for both even and odd N, σ tends to decrease with N. Additional investigation is required in order to understand the features of multipartite entanglement and in particular the large-N limit. As explained in [12], different scenarios are possible, depending on the behavior of σ/μ: if this ratio tends to zero with N, entanglement will tend to be well distributed among different bipartitions.

4 Conclusions

We analyzed the finite-size XX model on the circle. We diagonalized the Hamiltonian by defining a deformed Fourier transform that takes into account the periodic boundary conditions. We also studied the ground state of the chain, by focusing on the points of level crossings, that forerun the QPT in the thermodynamic limit, and defined a finite-size parameter that quantifies how rapidly this limit is approached. Finally, we looked at the properties of the multipartite entanglement of the ground state in terms of the distribution of bipartite entanglement. There is considerable interest in the study of entanglement for quantum spin chains, both in view of applications and because of their fundamental interest. Future activity will focus on the study of different models, with more general interactions and/or boundary conditions.

This work is supported by the European Community through the Integrated Project EuroSQIP and by the bilateral Italian Japanese Projects II04C1AF4E on "Quantum Information, Computation and Communication" of the Italian Ministry of Instruction, University and Research.

References

1. M.A. Nielsen, I.L. Chuang, *Quantum Computation and Quantum Information* (Cambridge University Press, Cambridge, 2000); G. Benenti, G. Casati, G. Strini, *Principles of Quantum Computation and Information* (World Scientific, Singapore, 2004)
2. S. Sachdev, *Quantum Phase Transitions* (Cambridge University Press, Cambridge, 1999)

3. E. Lieb, T. Schultz, D. Mattis, Ann. Phys. **16**, 407 (1961)
4. P. Pfeuty, Ann. Phys. **57**, 79 (1970)
5. L. Amico, R. Fazio, A. Osterloh, V. Vedral, Rev. Mod. Phys. (to be published) [quant-ph/0703044]; W.K. Wootters, Quant. Inf. Comp. **1**, 27 (2001)
6. X. Wang, Phys. Rev. A **66**, 034302 (2002); G.L. Kamta, A.F. Starace, Phys. Rev. Lett. **88**, 107901 (2002); M. Asoudeh, V. Karimipour, Phys. Rev. A **71**, 022308 (2005); M. Cao, S. Zhu, Phys. Rev. A **71**, 034311 (2005)
7. A. Osterloh, L. Amico, G. Falci, R. Fazio, Nature **416**, 608 (2002); G. Vidal, J.I. Latorre, E. Rico, A. Kitaev, Phys. Rev. Lett. **90**, 227902 (2003); F. Verstraete, M. Popp, J.I. Cirac, Phys. Rev. Lett. **92**, 027901 (2004); T. Roscilde, P. Verrucchi, A. Fubini, S. Haas, V. Tognetti, Phys. Rev. Lett. **93**, 167203 (2004); L. Campos Venuti, C. Degli Esposti Boschi, M. Roncaglia, Phys. Rev. Lett. **96**, 247206 (2006)
8. P. Štelmachovič, V. Bužek, Phys. Rev. A **70**, 032313 (2004) [arXiv:quant-ph/0410224]
9. N. Canosa, R. Rossignoli, Phys. Rev. A **75**, 032350 (2007)
10. V. Coffman, J. Kundu, W.K. Wootters, Phys. Rev. A **61**, 052306 (2000); A. Wong, N. Christensen, Phys. Rev. A **63**, 044301 (2001); D.A. Meyer, N.R. Wallach, J. Math. Phys. **43**, 4273 (2002)
11. P. Facchi, G. Florio, S. Pascazio, Phys. Rev. A **74**, 042331 (2006); Int. J. Q. Inf. **5**, 97 (2007)
12. G. Costantini, P. Facchi, G. Florio, S. Pascazio, J. Phys. A: Math. Theor. **40**, 8009 (2007)